

Size dependent hygroscopicity of levoglucosan and D-glucose aerosol nanoparticles

Ting Lei^{1,2}, Hang Su^{2,3}, Nan Ma⁴, Ulrich Pöschl², Alfred Wiedensohler⁵, Yafang Cheng¹

¹Minerva Research Group, Max Planck Institute for Chemistry, 55128 Mainz, Germany

²Multiphase Chemistry Department, Max Planck Institute for Chemistry, 55128 Mainz, Germany

³State Environmental Protection Key Laboratory of Formation and Prevention of Urban Air Pollution Complex, Shanghai Academy of Environmental Sciences, Shanghai 200233, China

⁴Institute for Environmental and Climate Research, Jinan University, 511443 Guangzhou, China

⁵Leibniz Institute for Tropospheric Research, 04318 Leipzig, Germany

Correspondence to: Yafang Cheng (yafang.cheng@mpic.de)

Abstract: The interaction between water vapor and aerosol nanoparticles is important in atmospheric processes. Hygroscopicity of sub-10 nm organic nanoparticles and their concentration-dependent thermodynamic properties (e.g., water activity) in the highly supersaturated concentration range are, however, scarcely available. Here we investigate the size dependence of hygroscopicity of organics (i.e., levoglucosan, D-glucose) in dry particle diameter down to 6 nm using a nano-hygroscopicity tandem differential mobility analyzer (nano-HTDMA). Our results show that there is only a weak size dependent hygroscopic growth of both levoglucosan and D-glucose nanoparticles with diameters down to 20 nm. In the diameter range smaller than 20 nm (down to 6 nm), we observed a strong size-dependent hygroscopic growth for D-glucose nanoparticles. The hygroscopic growth factors cannot be determined for levoglucosan below 20

23 nm due to its evaporation. In addition, we compare hygroscopicity measurements for levoglucosan
24 and D-glucose nanoparticles with the E-AIM (standard UNIFAC), the ideal solution theory, and
25 DKA predictions, respectively. The ideal solution theory describes well the measured hygroscopic
26 growth factors of levoglucosan with diameters down to 20 nm and D-glucose nanoparticles with
27 diameters higher than 60 nm, respectively, while the E-AIM (standard UNIFAC) model can
28 successfully predict the growth factors of D-glucose nanoparticles with diameters from 100 down
29 to 6 nm at RH above 88-40 % (e.g., at RH above 88 % for 100 nm D-glucose, at RH above 40 %
30 for 6 nm D-glucose). The use of the DKA method leads to a good agreement with measured
31 hygroscopic growth factors of D-glucose aerosol nanoparticles with diameters from 100 down to
32 6 nm. Predicted water activity for these aqueous organic solutions (i.e., levoglucosan, D-glucose)
33 from different parameterization methods agrees well with observations in the low solute
34 concentration range ($< 20 \text{ mol kg}^{-1}$), and start to deviate from observations in the high solute
35 concentration ($> 20 \text{ mol kg}^{-1}$).

36

37 **1 Introduction**

38 Organic aerosol nanoparticles play an important role in new particle formation, subsequent
39 condensation and coagulation growth, cloud condensation nuclei (CCN), and thus in affecting
40 visibility degradation, radiative forcing, and climate (Chylek and Coakley, 1974; Charlson et al.,
41 1992; Dusek et al., 2010; Cheng et al., 2012; Zhang et al., 2012; Kulmala et al., 2013). Both growth
42 of nanoparticles and their ability to act as CCN are directly related to its hygroscopicity that
43 describes the interaction between organic nanoparticles and water vapor (Köhler, 1936;
44 Kreidenweis et al., 2005; Su et al., 2010; Cheng et al., 2015; Wang et al., 2015). However, current
45 knowledge of hygroscopicity of sub-10 nm organic nanoparticles and their concentration-

46 dependent thermodynamic properties (e.g., water activity) in the highly supersaturated
47 concentration range is scarcely available.

48 Levoglucosan aerosol nanoparticles have attracted increasing interest in recent years (Simoneit et
49 al., 1999; Mochida and Kawamura, 2004; Mikhailov et al., 2009; Elias et al., 2010; Lei et al., 2014,
50 2018; Bhattarai et al., 2019) due to relative stability and high emission factors, which are
51 considered as an ideal tracer for characterization and quantification the biomass burning (Fraser
52 and Lakshmanan, 2000). Also, levoglucosan is typically the most abundant species in wood
53 burning aerosols, which contributes substantially (16.6–30.9% by mass) to the total organics in
54 PM_{2.5} (Mochida and Kawamura, 2004; Bhattarai et al., 2019). D-glucose, a hydrolysis product of
55 cellulose and levoglucosan, is a major pyrolysis product of wood (Mochida and Kawamura, 2004;
56 Bhattarai et al., 2019; Mikhailov and Vlasenko., 2020). Hygroscopicity of levoglucosan and D-
57 glucose substances is thus important in reproducing the overall hygroscopic behavior of the real
58 biomass burning aerosol particles (Bhandari and Bareyre. 2003; Mochida and Kawamura, 2004;
59 Chan et al., 2005; Koehler et al., 2006; Peng et al., 2010; Mikhailov and Vlasenko., 2020). For
60 example, a small difference in the hygroscopicity parameter (κ) between measured data of model
61 mixtures including levoglucosan and ammonium sulfate in the laboratory using HTDMA and
62 biomass burning aerosol particles in the field using CCN activity measurement due to the similar
63 O: C ratios of levoglucosan and ammonium sulfate mass fractions used in model mixtures when
64 experimental κ data from sub- and supersaturated water vapor conditions are compared (Bhandari
65 and Bareyre. 2003; Mochida and Kawamura, 2004; Chan et al., 2005; Koehler et al., 2006; Peng
66 et al., 2010; Pöhlker et al., 2016; Lei et al., 2018; Mikhailov and Vlasenko., 2020). Most of the
67 previous lab studies have focused on investigation of the hygroscopic behavior of 100-nm
68 levoglucosan and D-glucose aerosol nanoparticles, which mainly utilized the humidified tandem

69 differential mobility analyzers (DMAs) (Mikhailov et al., 2004; Mochida and Kawamura, 2004;
70 Koehler et al., 2006; Lei et al., 2014; 2018). For example, Mochida and Kawamura (2004) observed
71 that 100-nm levoglucosan and D-glucose aerosol nanoparticles uptake/release water continuously
72 in both deliquescence and efflorescence modes, respectively. To our knowledge, there are no phase
73 transitions for these organic aerosol nanoparticles in both deliquescence and efflorescence
74 processes.

75 Early studies showed that the hygroscopicity and solubility of inorganic aerosols, such as
76 ammonium sulfate (AS) and sodium chloride (NaCl), exhibited a strong size dependence (Cheng
77 et al., 2015). Firstly, hygroscopic diameter growth factors of AS, NaCl as well as Na₂SO₄
78 nanoparticles are found to decrease with size decreases in both deliquescence and efflorescence
79 modes (Biskos et al., 2006a, b, c, Lei et al., 2020). Secondly, there is no significant difference in
80 the deliquescence relative humidity (DRH) and the efflorescence relative humidity (ERH) between
81 AS nanoparticles with dry diameters of 6 and 60 nm (Biskos et al., 2006b; Lei et al., 2020), while
82 a pronounced size dependence of the DRH of NaCl is up to 10 % RH between dry diameters of 6
83 and 60 nm (Biskos et al., 2006a). The behaviors of change of phase transition RH and
84 concentrations of Na₂SO₄ are between NaCl and AS (Lei et al., 2020). However, there are very few
85 lab studies on investigating hygroscopicity (g_f , DRH, ERH) of organic aerosol nanoparticles in sub-
86 10 nm size range (Wang et al., 2017). It is not clear how the size effect influences the hygroscopic
87 growth of organics, especially those without DRH and ERH. Besides technique limitation (Lei et
88 al., 2020; Wang et al., 2017), another reason is the high diffusion of sub-100 nm organic
89 nanoparticles, especially in the sub-10 nm size range, which results in nanoparticle losses in the
90 HTDMA system (Seinfeld and Pandis, 2006).

91 Thermodynamic model is widely used to predict the hygroscopic growth factor of organic aerosol
92 particles as a function of RH (Bhandari and Bareyre. 2003; Chan et al., 2005; Koehler et al., 2006;
93 Peng et al., 2010). The thermodynamic model needs thermodynamic data such as water activity,
94 liquid-vapor interfacial energy (surface tension), and density of organic aqueous solutions (Tang
95 and Munkelwitz, 1994; Tang 1996; Pruppacher and Klett, 1997; Clegg et al., 1998). Because
96 nanodroplets can become more highly supersaturated where no thermodynamic data are available,
97 it makes the current thermodynamic model difficult or impossible to predict the hygroscopic
98 behavior of organic aerosol nanoparticles. Cheng et al. (2015) pointed out that size effect might be
99 taken models into account. By measuring the hygroscopic growth factor of organic nanoparticles
100 (e.g., levoglucosan and D-glucose) of different sizes, we may be able to retrieve these
101 thermodynamic data using a Differential Köhler Analysis (DKA) method (Cheng et al., 2015). This
102 will further help us to understand the new particle formation, transportation, and their interactions
103 between water molecules.

104 In this study, we investigate the hygroscopic growth factors of levoglucosan and D-glucose
105 nanoparticles in size down to 6 nm using a nano-hygroscopic tandem differential mobility analyzer
106 (nano-HTDMA, Lei et al., 2020). Moreover, we compare our measurement data with model
107 prediction from the Extended Aerosol Inorganic Model (E-AIM (standard UNIFAC)) (Clegg et al.,
108 2001; Clegg and Seinfeld, 2006; available online: <http://www.aim.env.ac.uk/aim/aim.php>), the
109 ideal solution theory, and DKA. In addition, the use of the DKA method is to calculate
110 thermodynamic properties (e.g., water activity) of D-glucose nanodroplets in the highly
111 supersaturated concentration range and then to compare with KD-derived data (KD=Kreidenweis),
112 thermodynamic property data from Köhler (Kreidenweis et al., 2005), E-AIM (standard UNIFAC)
113 model, and references, respectively.

114

115 **2 Methodology**

116 **2.1 Experimental methods**

117 **2.1.1 Nanoparticle generation**

118 An electrospray is employed to generate levoglucosan and D-glucose aerosol nanoparticles of 6, 8,
119 10, and 15 nm using 2, 3, 5, and 10 mM aqueous solutions with 50 % volume fraction of a 20 mM
120 ammonium acetate buffer solution (Chen et al., 2005; Wang et al., 2015), respectively. The
121 generated nanoparticles are diluted by mixing with dry and filtered N₂ (1 l/min) and CO₂ (0.1 l/min),
122 bringing aerosol nanoparticles to a dry RH state ($\leq 2\%$ RH). Subsequently, aerosol nanoparticles
123 pass through a Po²¹⁰ neutralizer to reach the equilibrium charge distribution (Wiedensohler 1986).
124 In order to avoid blocking the 25- μ m capillary tube in the electrospray with high solution
125 concentration, the aerosol nanoparticles with diameters of 60-100 and 20 nm are generated by an
126 atomizer with a 0.05 and 0.01 wt % organic solution (i.e., levoglucosan and D-glucose),
127 respectively. The chemical substances and their physical properties are characterized in Table S1.
128 These solutions are prepared with distilled and de-ionized million-Q water (resistivity of 18.2 M Ω
129 cm at 298.15 K). Note that the size selected by the nano-DMA1 should be the right part of peak
130 diameter of the number size distribution of the generated nanoparticles, which minimizes the
131 influence of the multiple charged nanoparticles in hygroscopicity measurements. This is to ensure
132 that we could have as many particles as possible to compensate for the strong loss of very small
133 particles in the whole humidification system.

134 **2.1.2 Nano-HTDMA setup**

135 Figure 1 shows a schematic of the nano-HTDMA system for investigating the hygroscopic
136 behavior of aerosol nanoparticles, especially in the sub-10 nm size range. The detailed description,
137 calibration, and validation of nano-HTDMA setup have been reported in the previous paper (Lei et
138 al., 2020). In brief, the polydisperse aerosol nanoparticles pass through a silica gel diffusion dryer
139 and a Nafion gas dryer (TROPOS Model ND.070, Length 60 cm). The dry aerosol nanoparticles
140 at RH below 10 % are charged by a Kr⁸⁵ bipolar charger and then enter the first nano-differential
141 mobility analyzer (nano-DMA1, TROPOS Model Vienna-type short DMA), where a monodisperse
142 distribution of nanoparticles with the desired dry diameter is selected. The monodispersed
143 nanoparticles subsequently are exposed to the different RH conditions, which can be set to
144 deliquescence mode (from low RH to high RH for measuring deliquescence) or efflorescence mode
145 (from the high RH to low RH for measuring efflorescence). In the deliquescence mode, the dry
146 aerosol nanoparticles are gradually humidified to a target RH through a Nafion humidifier (NH-1,
147 TROPOS Model ND.070, Length 60 cm). In the efflorescence mode, after deliquescence of aerosol
148 nanoparticles with RH above 97% in a Nafion humidifier (NH-2: Perma Pure Model MH-110,
149 Length 30 cm), the deliquesced aerosol nanoparticles are stepwise dried to a target RH in NH-1.
150 The number size distribution of the humidified nanoparticles is then measured by a nano-
151 differential mobility analyzer (nano-DMA2) at a target RH through a Nafion humidifier (NH-3,
152 Perma Pure Model PD-100) coupled with an ultrafine condensation particle counter (CPC, TSI,
153 model no. 3776). To have the uniform RH within the nano-DMA2 for the accurate determination
154 of hygroscopicity (g_f , DRH, ERH) of aerosol nanoparticles, the difference between the sheath flow
155 RH (RH_s) and the aerosol flow RH (RH_a) upstream of the nano-DMA2 is kept <1 %. Most
156 importantly, the temperature difference between inlet and outlet of the nano-DMA2 is maintained
157 below 0.2 °C during the measurements. In addition, the residence time (e.g., 5.4 s: between the

158 humidifier and the nano-DMA2; 0.07 s: deliquescence for aerosol nanoparticles) is sufficient for
159 water-soluble aerosol nanoparticles to equilibrate with water vapor at a given RH and to occur
160 solid-liquid phase transition (Kerminen 1997; Duplissy et al., 2005; Raoux et al., 2007),
161 respectively.

162 **2.2 Theory and modeling methods**

163 **2.2.1 Köhler theory**

164 The fractional ambient relative humidity ($\frac{RH}{100}$) over a spherical droplet in equilibrium with the
165 environment is described by Köhler equation (Köhler 1936):

$$166 \quad \frac{RH}{100} = a_w \exp\left(\frac{4\sigma_{sol}v_w}{RTG_f D_s}\right) \quad (1)$$

167 where a_w is the water activity of the solution droplet, σ_{sol} is the liquid-vapor interfacial energy of
168 solution droplet (also called surface tension), v_w is the partial molar volume of water, R is the
169 universal gas constant, T is the temperature, G_f is the diameter growth factor of aerosol particles,
170 and D_s is the dry diameter of spherical aerosol particles. The hygroscopic growth curve (G_f vs RH)
171 is estimated based on the assumptions in models or theories described in the following sections
172 (2.2.2-2.2.3).

173 **2.2.2 Water activity**

174 The expression for water activity used in the Simplified Kohler Theory (SKT) assumes the droplet
175 contains n_w moles of water and n_s moles of nonvolatile solute.

$$176 \quad a_w = \frac{n_w}{n_w + v n_s} \quad (2)$$

177 v is the number of ions of solute present in solution ($v=1$ for organic composition). This expression
178 has been applied to the diluted solution (Kreidenweis et al., 2005; Koehler et al., 2006).

179 The following KD expression proposed by Kreidenweis et al. (2005) (KD= Kreidenweis) is to
180 present the relationship between a_w and G_f determined in hygroscopic growth measurements:

$$181 \quad G_f = \left[1 + (a + b * a_w + c * a_w^2) \frac{a_w}{1-a_w} \right]^{\frac{1}{3}} \quad (3)$$

182 The coefficients a, b, and c for organic solution droplet in this study from Lei et al. (2014, 2018)
183 and Estillore et al. (2017) as shown in Table S2.

184 Differential Köhler analysis (DKA) proposed by Cheng et al. (2015) is theoretically based on
185 Köhler equation (Köhler, 1936) to determine water activity by measuring hygroscopic growth
186 factors of aerosol nanoparticles in different sizes.

$$187 \quad a_w = \frac{s_{w1}^{\left(\frac{D_{s1}}{D_{s1}-D_{s2}}\right)}}{s_{w2}^{\left(\frac{D_{s2}}{D_{s1}-D_{s2}}\right)}} \quad (4)$$

188 where s_{w1} and s_{w2} are water saturation ratio measured at the same g_f but at the different initial dry
189 diameters (D_{s1}, D_{s2}), respectively. Using the DKA method can calculate the water activity in the
190 highly supersaturated concentration range.

191 **2.2.3 Growth factor**

192 For ideal solution, the hygroscopic curve can be estimated assuming that the water activity a_w of
193 the solution containing non-volatile and non-electrolyte solute component is equal to the molar
194 ratio of water in the solution. Here, the partial molar volume of pure water in the solution is equal
195 to the molar volume of pure water. Since the hygroscopic diameter growth factor measurements

196 are on volume basis using nano-HTDMA system, the expression of G_f as a function of molar ratio
197 (x_j), molar mass (M_j), and mass density (ρ_j) of components j as follows:

$$198 \quad G_f = \left[\frac{\sum_j \left(x_j M_j \frac{1}{\rho_j} \right)}{\sum_{j,j \neq w} \left(x_j M_j \frac{1}{\rho_j} \right)} \right]^{\frac{1}{3}} \quad (5)$$

199 The hygroscopic growth curve of aerosol particles is commonly evaluated from Extend-Aerosol
200 Inorganic Model (E-AIM). It is a thermodynamic equilibrium model used for calculating phase
201 partitioning (gas/liquid/solid). Most importantly, the E-AIM mode can model thermodynamic
202 properties (e.g., water activity, liquid-vapor interfacial energy, and solution density) in the highly
203 supersaturated concentration solution (Dutcher et al., 2013). Also, the standard universal quasi-
204 chemical functional group activity coefficients (UNIFAC) within E-AIM can be used to predict
205 a_w , σ_{sol} , and ρ_{sol} of organic aqueous solution (Fredenslund et al., 1975; Hansen et al., 1991). Note
206 that the E-AIM calculations based on the standard UNIFAC group contribution method predict
207 hygroscopic growth factors of organic aerosol particles. (i.e., E-AIM model (standard UNIFAC))
208 growth curve as a function of RH is based on Eq. (1) and Eq. (6).)

$$209 \quad G_f = \left(\frac{\rho_s}{x_s \rho_{sol}} \right)^{\frac{1}{3}} \quad (6)$$

210 ρ_s and ρ_{sol} are the density of solute and solution, respectively, and x_s is the solute mass fraction.

211

212 **3 Results and discussion**

213 **3.1 Levoglucosan**

214 **3.1.1 Concentration-dependent water activity of levoglucosan solution**

215 By applying a water activity parameterization model (KD, Eq. 3) to measured growth factors of
216 levoglucosan aerosol nanoparticles with diameters from 20 to 100 nm using a nano-HTDMA, as
217 shown in Fig. 2, we obtain water activity of aqueous levoglucosan nanoparticles with molality up
218 to 140 mol kg⁻¹. Chan et al. (2005) levitated single particles of ~10 μm levoglucosan at the different
219 RHs in an electrodynamic balance for mass measurements, and reported water activity data for
220 aqueous droplets with molality up to 14 mol kg⁻¹. These water activity data are compared with
221 predictions from the Köhler (Kreidenweis et al., 2005, Eq. 2) and the E-AIM model, respectively.
222 A good agreement between KD-derived water activity and Köhler indicates these aerosol particles
223 are aqueous droplets with molality less than 20 mol kg⁻¹. However, a derivation of SKT from the
224 KD-derived water activity is observed as the molality increases from 20 to 120 mol kg⁻¹, indicating
225 levoglucosan nanoparticles become highly supersaturated. Also, a discrepancy exists between KD-
226 derived data and E-AIM model prediction. For DKA-derived water activity calculations, a strong
227 size dependence of the hygroscopic growth factors is needed for aerosol nanoparticles in the
228 different sizes, which is not the case for the hygroscopic measurements of levoglucosan
229 nanoparticles.

230 **3.1.2 Size dependent hygroscopicity of levoglucosan nanoparticles**

231 Black solid squares in Fig. 3 shows the measured humidogram of 100-nm levoglucosan
232 nanoparticles in both deliquescence and efflorescence modes. Levoglucosan nanoparticles uptake
233 water continuously from 5 % to 90 % RH. Also, they gradually release water as RH decreases
234 down to 5 %. The hygroscopic growth factors of levoglucosan nanoparticles in deliquescence and
235 efflorescence modes overlap. For example, the hygroscopic growth factors of levoglucosan
236 nanoparticles at 80 % RH, 87 % RH are 1.16, 1.23, respectively, in the deliquescence mode, very
237 close to the corresponding values in the efflorescence mode are 1.15, 1.22 (shown in Fig. S1),

238 suggesting that growing and shrinking of particles are in equilibrium with water vapor surrounding
239 moisture conditions. No prompt phase transitions of levoglucosan nanoparticles are observed in
240 both deliquescence and efflorescence modes. A similar non-prompt phase transition of
241 levoglucosan nanoparticles was observed in the previous studies (Mochida and Kawamura, 2004;
242 Chan et al., 2005; Svenningsson et al., 2006; Mikhailov et al., 2008; Lei et al., 2014, 2018). This
243 study is in good agreement with most of reference results, but there is a difference in the
244 hygroscopic growth factor of levoglucosan nanoparticles between Mikhailov et al. (2008) and this
245 study. The reason is that Mikhailov et al. (2008) used minimum mobility diameter measured in the
246 deliquescence and efflorescence modes instead of the initial dry mobility diameter measured in the
247 deliquescence or efflorescence modes to calculate the hygroscopic growth factor of levoglucosan
248 nanoparticles, which could lead to the higher hygroscopic growth factors of levoglucosan
249 nanoparticles than those of this study.

250 Figure 4 shows measured size-resolved hygroscopic growth factors of levoglucosan nanoparticles
251 against RH up to 90 %. There is a weak size dependence of hygroscopic growth factors of
252 levoglucosan nanoparticles with diameters down to 20 nm in both deliquescence and efflorescence
253 modes. E.g., a slight difference in hygroscopic growth factor between 100 and 20-nm levoglucosan
254 nanoparticles is ~ 0.02 at 88 % RH. In addition, E-AIM (standard UNIFAC) model and ideal
255 solution theory are used to predict our measurement results as shown in Fig. 4a and 4b, respectively.
256 E-AIM (standard UNIFAC) model is applied to estimate the hygroscopic growth of organic aerosol
257 nanoparticles according to UNIFAC group contribution method. Ideal solution theory is used to
258 describe water absorption of the ideal/diluted aqueous solution nanodroplets. Due to consideration
259 of Kelvin effect in model and theory, these model predictions are expected to present a size
260 dependence of growth factors of nanoparticles in size from 100 down to 20 nm. For example, as

261 shown in Fig. 4a, the thermodynamic equilibrium model (E-AIM (standard UNIFAC)) shows a
262 weak size dependence of the growth factors of levoglucosan nanoparticles with diameters 100, 60,
263 and 20 nm at low RH but a strong size dependence of growth factors at RH above 70 %. However,
264 the calculated growth factors of nanoparticles down to 20 nm in size are deviated from the
265 measured growth factors of levoglucosan nanoparticles at RH below 80 %, which is similar to the
266 observation of 100-nm levoglucosan hygroscopicity prediction from previous studies (Lei et al.,
267 2014, 2018). Lei et al. (2014, 2018) explained that the possible reason for this discrepancy is that
268 the E-AIM (standard UNIFAC) predictions are not suitable for organic compounds with the
269 strongly polar functional groups in series (Fredenslund et al., 1975; Hansen et al., 1991). Since
270 levoglucosan contains three OH groups in series, thus, thermodynamic properties (e.g., water
271 activity, surface tension) in E-AIM (standard UNIFAC) are more likely to be invalid for
272 levoglucosan system. However, a good agreement of growth factors of levoglucosan with
273 diameters 100, 60, and 20 nm is observed between measurements and predictions by ideal solution
274 theory as shown in Fig. 4b.

275 The hygroscopic growth for sub-20 nm levoglucosan nanoparticles cannot be determined with the
276 nano-HTDMA system because we observed significant evaporation of the dry particles in the
277 measurement system. Figure 5a-b shows the measured peak diameter of normalized size
278 distribution scanned by the nano-DMA2 and nano-DMA1 for sub-20 nm levoglucosan
279 nanoparticles. It is obvious that the size of nanoparticles in DMA2 is smaller than that in DMA1,
280 corresponding to a decrease of 22% to 50% of 15-nm and 10-nm levoglucosan nanoparticles,
281 respectively, indicating significant evaporation of these small levoglucosan nanoparticles in the
282 system. To test this hypothesis, we estimate the ratio of gas-phase concentration to the total
283 concentration of the generated levoglucosan nanoparticles in the different sizes. Firstly, the

284 calculated gas-phase concentration of levoglucosan is based on the Kelvin equation and ideal gas
285 equation (Eq. S1&2, SI. S1). Figure 5c shows the vapor saturation ratio of levoglucosan as
286 nanodroplet diameter increases from 0 to 100 nm. The inset in Fig. 5c is an enlarged view (black
287 open square) of vapor saturation ratio of levoglucosan as a function of nanodroplet diameters below
288 20 nm. Levoglucosan is semi-volatile at ambient condition (Hennigan et al., 2010). Due to Kelvin
289 effect, sub-20 nm levoglucosan aerosol particles become more volatile. Secondly, the total
290 concentration of levoglucosan particles is estimated by Eq. (S3). Thus, the results of the ratio of
291 gas-phase concentration (m_g) to the total concentration (m_t) have been shown in Fig. 5d and Table
292 S3 for levoglucosan nanoparticles in the diameter range from 10 to 100 nm. It shows a slight
293 increase in the calculated ratio (m_g/m_t) for levoglucosan aerosol nanoparticles with diameters from
294 100 down to 20 nm. However, the ratio of gas-phase concentration to the total concentration is
295 dramatically enhanced for sub-20 nm levoglucosan aerosol nanoparticles, which is consistent with
296 measurement observations, indicating the larger impact of evaporation of sub-20 nm levoglucosan
297 nanoparticles on the measurement results. Therefore, there is an obvious partial levoglucosan
298 evaporation from DMA1 to DMA2 within several seconds.

299 **3.2 D-glucose**

300 **3.2.1 Concentration-dependent water activity of D-glucose solution**

301 Figure 6 shows the DKA-derived water activity of aqueous D-glucose nanodroplets with diameters
302 from 6 nm to 100 nm with molality up to 1000 mol kg⁻¹ (Cheng et al., 2015, Eq. 4). Here, by
303 comparing with KD-derived water activity, Köhler, E-AIM model, and observation from literatures
304 (Comesaña et al., 2001; Peng et al., 2001; Bhandari and Bareyre, 2003; Ferreira et al., 2003), a
305 good agreement among them is observed in the solute concentration below 20 mol kg⁻¹. However,

306 there is a disagreement between water activity results in the highly supersaturated concentration
307 range ($> 20 \text{ mol kg}^{-1}$).

308 **3.2.2 Size dependent hygroscopicity of D-glucose nanoparticles**

309 Figure 7 shows the measured hygroscopic growth factors of 100-nm D-glucose nanoparticles as a
310 function of RH. No significant difference in the hygroscopic growth factor of 100-nm D-glucose
311 nanoparticles is found between deliquescence and efflorescence measurement modes (Fig. S2). For
312 example, the measured growth factors of D-glucose nanoparticles at 81 % RH, 88 % RH are 1.16,
313 1.25 in the deliquescence mode, respectively, in good agreement with results in the efflorescence
314 mode ($g_f=1.17$ at 81 % RH, $g_f=1.26$ at 88 % RH shown in Fig. S2). Also, measured hygroscopic
315 growth factors of 100-nm D-glucose are consistent with results from previous studies (Mochida
316 and Kawamura, 2004; Chan and Chan, 2005; Suda and Petters, 2013; Estillore et al., 2017;
317 Mikhailov and Vlasenko, 2020). For example, Mikhailov and Vlasenko, (2020) investigated the
318 hygroscopic behavior of 100-nm D-glucose aerosol particles using a HHTDMA in deliquescence,
319 efflorescence, and restructuring modes of operation, respectively. A clear morphology effect on
320 the hygroscopicity of D-glucose aerosol particles is observed in the RH range from 2 % to 96 %
321 RH. No prompt phase transitions are observed in both deliquescence and efflorescence
322 measurement modes. Estillore et al. (2017) observed a slightly amorphous structure of D-glucose
323 particles under ambient conditions using an atomic force microscopy and D-glucose particles grow
324 through gradual water uptake where the solid-liquid phase transition is non-discrete. Thus, a
325 continuous growth/shrink of diameter in both deliquescence and efflorescence modes is explained
326 by the lack of crystallization of D-glucose nanoparticles upon drying to low RH below 10 %.

327 Figure 8a shows the size dependence of measured hygroscopic growth factors of D-glucose
328 nanoparticles in the size range from 6 to 100 nm, with differences in growth factor up to 0.14

329 between 100-nm and 6-nm nanoparticles at 90 % RH (Fig. S2). A weak size dependence on the
330 hygroscopic growth factors of D-glucose nanoparticles is observed in the size range from 20 to 100
331 nm, which is similar to observation for levoglucosan nanoparticles with diameters down to 20 nm.
332 However, there is a strong size-dependent growth factor of D-glucose nanoparticles with diameters
333 from 6 to 20 nm, especially at high RH, i.e., $RH > \sim 80\%$. There is no evident difference in
334 hygroscopic growth factors of D-glucose nanoparticles at RH below 80 % in size range from 6 to
335 100 nm. The reason that the growth factor shows size dependence only in the regime of hygroscopic
336 growth ($RH > 80\%$), and not in the regime of water adsorption ($RH < 80\%$) has not been explained
337 before. Our hypothesis is that the distinct behaviors between high RH and low RH region can be
338 attributed to the distinct size effect on the hygroscopic growth and adsorption, i.e., the growth factor
339 shows size dependence only in the regime of hygroscopic growth ($RH > 80\%$), and not in the
340 regime of water adsorption ($RH < 80\%$). Figure 8b further shows the clear change in the
341 hygroscopic growth factor of D-glucose aerosol nanoparticles with diameters from 100 down to 6
342 nm at 87 % RH. The hygroscopic growth factor of D-glucose nanoparticles is almost unchanged
343 with diameters from 20 to 100 nm. However, a markedly increase in the hygroscopic growth factor
344 of D-glucose aerosol nanoparticles is observed as size increases from 6 to 20 nm. E-AIM model
345 predict well the measured hygroscopic growth factors of D-glucose with diameters smaller than 15
346 nm at 87 % RH, while ideal solution theory agrees with hygroscopic measurement results of D-
347 glucose with diameters higher than 60 nm at the same RH. The use of DKA methods leads to a
348 good agreement between measurements and model predictions.

349 The measured hygroscopic growth factors of D-glucose nanoparticles with diameters of 6 and 100
350 nm are compared with the model and theory shown in Fig. 9, Fig. S3, and Fig. S4, respectively.
351 Ideal solution theory is applied to predict the hygroscopic growth factor of organics in the ideal

352 solution. Figure 9a and Fig. S3 show that the measured growth factors of 100-nm D-glucose
353 nanoparticles are lower than predicted growth factors from E-AIM (standard UNIFAC) model,
354 especially at RH below 85 %. Also, E-AIM (standard UNIFAC) model could predict well the
355 measured hygroscopic growth factor of 6-nm D-glucose aerosol nanoparticles at RH above 40 %
356 shown in Fig. 9a and Fig. S3. The possible reason for discrepancies between E-AIM (standard
357 UNIFAC) model and measurements is inaccurate thermodynamic parameters (e.g., water activity,
358 surface tension) estimated by the E-AIM (standard UNIFAC) model without consideration
359 intramolecular interaction (Fredenslund et al., 1975; Hansen et al., 1991; Fredenslund and Sørensen,
360 1994; Mochida and Kawamura, 2004). D-glucose contains five OH groups in series, hydrogen
361 bond could potentially exist and affects the E-AIM (standard UNIFAC) model-measurement
362 agreement for D-glucose aerosol nanoparticles system (Mochida and Kawamura, 2004; Lei et al.,
363 2014, 2018). Using of ideal solution theory is to predict the hygroscopic curve of D-glucose
364 nanoparticles with diameters of 6-100 nm shown in Fig. 9b and Fig. S3. There is a good agreement
365 between measured growth factors of 100-nm D-glucose and ideal theory predictions. This suggests
366 that thermodynamic parameters (e.g., water activity, surface tension, and solution density) assumed
367 by the ideal solution theory are accurate to use in Eq. (1) and (2) for predicting the hygroscopic
368 curve of D-glucose nanoparticles with large sizes (e.g., 60, 100 nm). However, an underestimation
369 of growth factors of 6-nm D-glucose nanoparticles has been shown in Fig. 9b and Fig. S3 by ideal
370 solution theory prediction at RH above 30 %. The possible reason is the unfavorable assumption
371 of ideal solution theory. As D-glucose size decreases from 20 to 6 nm, D-glucose nanodroplets
372 could be highly supersaturated in concentration compared to the dilution solution. However, the
373 current thermodynamic models (e.g., E-AIM) mostly rely on the concentration-dependent
374 thermodynamic properties (such as water activity) derived from the measurements of large aerosol

375 particles or even bulk samples (Tang and Munkelwitz, 1994; Tang, 1996; Pruppacher and Klett,
376 1997; Clegg et al., 1998). They are thus difficult or impossible to apply to describe the hygroscopic
377 behavior of sub-10 nm nanoparticles, which can often be supersaturated in concentration compared
378 to bulk solutions (Cheng et al., 2015; Wang et al., 2018). Thus, nanosize effect on these
379 thermodynamic properties has been taken into account the models and theories (Cheng et al., 2015).
380 Combination of DKA methods and hygroscopic measurements of aerosol nanoparticles in the
381 different sizes can use to determine the thermodynamic properties (e.g., water activity) in the highly
382 supersaturated concentration range (Cheng et al., 2015). Therefore, as shown in Fig. 9c and Fig.
383 S4, the use of the DKA method leads a good agreement with the measured hygroscopic growth
384 factors of Glucose nanoparticles with diameters from 100 down to 6 nm.

385

386 **4 Conclusions**

387 In this study, we investigate the hygroscopic behavior of levoglucosan and D-glucose nanoparticles
388 with diameters down to 6 nm using a nano-HTDMA. Due to the larger impact of evaporation of
389 sub-20 nm levoglucosan nanoparticles in the nano-HTDMA system, we measure hygroscopic
390 growth factor of levoglucosan with diameters down to 20 nm. There is a weak size dependence of
391 hygroscopic growth factor of levoglucosan and D-glucose with diameters down to 20 nm, while a
392 strong size dependence of the hygroscopic growth factor of D-glucose has been clearly observed
393 in the size range from 6 to 20 nm. No prompt phase transitions occur in both deliquescence and
394 efflorescence modes for both levoglucosan and D-glucose nanoparticles. By comparing with the
395 KD-derived water activity, Köhler, E-AIM model, and DKA-derived data, the predicted water
396 activity of aqueous organic solution (levoglucosan and D-glucose) is consistent with observation
397 data from references in the low solute concentration ($< 20 \text{ mol kg}^{-1}$) but failed in the solute

398 concentration ($> 20 \text{ mol kg}^{-1}$). In addition, ideal solution theory predicts well the hygroscopic
399 behavior of two specific organics with diameters higher than 60 nm (levoglucosan and D-glucose),
400 while hygroscopic growth factor of D-glucose down to 6 nm in size is in good agreement with E-
401 AIM (standard UNIFAC) model prediction at high RH. The use of the DKA method leads to a
402 good agreement with measured hygroscopic growth factor of glucose nanoparticles with diameters
403 from 100 down to 6 nm.

404

405 **Data availability**

406 Reader who are interested in the data should contact Yafang Cheng (Yafang.cheng@mpic.de).

407 **Competing interests**

408 Some authors are members of the editorial board of journal Atmospheric Chemistry Physics. The
409 peer-review process was guided by an independent editor, and the authors have also no other
410 competing interests to declare

411 **Acknowledgement**

412 This study was supported by the Max Planck Society (MPG) and Leibniz Society. T.L.
413 acknowledges the support from China Scholarship Council (CSC). Y. C. would like to
414 acknowledge the Minerva Program of MPG.

415 **Author contributions:** Y.C. and H.S. designed and led the study. T.L. performed the experiments.
416 All co-authors discussed the results and commented on the manuscript. T.L. wrote the manuscript
417 with input from all co-authors

418 **4 References**

419 Andreae, M. O. and Gelencsér, A.: Black carbon or brown carbon? The nature of light-absorbing
420 carbonaceous aerosols, *Atmos. Chem. Phys.*, 6, 3131–3148, [https://doi.org/10.5194/acp-6-](https://doi.org/10.5194/acp-6-3131-2006)
421 3131-2006, 2006.

422 Bhandari, B. and Bareyre, I.: Estimation of crystalline phase present in the glucose crystal–solution
423 mixture by water activity measurement, *LWT - Food Science and Technology*, 36, 729-733,
424 2003.

425 Bhattarai, H., Saikawa, E., Wan, X., Zhu, H., Ram, K., Gao, S., Kang, S., Zhang, Q., Zhang, Y.,
426 Wu, G., Wang, X., Kawamura, K., Fu, P., and Cong, Z.: Levoglucosan as a tracer of biomass
427 burning: Recent progress and perspectives, *Atmos. Res.*, 220, 20–33, 2019.

428 Biskos, G., Malinowski, A., Russell, L. M., Buseck, P. R., and Martin, S. T.: Nanosize effect on
429 the deliquescence and the efflorescence of sodium chloride particles, *Aerosol Sci. Technol.*,
430 40, 97-106, 2006a.

431 Biskos, G., Paulsen, D., Russell, L. M., Buseck, P. R., and Martin, S. T.: Prompt deliquescence and
432 efflorescence of aerosol nanoparticles, *Atmos. Chem. Phys.*, 6, 4633–4642,
433 <https://doi.org/10.5194/acp-6-4633-2006>, 2006b.

434 Biskos, G., Russell, L. M., Buseck, P. R., and Martin, S. T.: Nanosize effect on the hygroscopic
435 growth factor of aerosol particles, *Geophys. Res. Lett.*, 33, L07801,
436 [doi:10.1029/2005GL025199](https://doi.org/10.1029/2005GL025199), 2007.

437 Bohren, C. and Huffmann, D.: Absorption and scattering of light by small particles, Wiley-VCH,
438 New York, USA, 2004.

439 Bzdek, B. R., Zordan, C. A., Luther, G. W., and Johnston, M. V.: Nanoparticle Chemical
440 Composition During New Particle Formation, *Aerosol Science and Technology*, 45, 1041-
441 1048, 2011.

442 Chan, M. N., Choi, M. Y., Ng, N. L., and Chan, C. K.: Hygroscopicity of water-soluble organic
443 compounds in atmospheric aerosols: Amino acids and biomass burning derived organic species,
444 *Environ. Sci. Technol.*, 39, 1555-1562, 2005.

445 Chan, M. N. and Chan, C. K.: Mass transfer effects in hygroscopic measurements of aerosol
446 particles, *Atmos. Chem. Phys.*, 5, 2703–2712, <https://doi.org/10.5194/acp-5-2703-2005>, 2005.

447 Charlson, R. J., Schwartz, S. E., Hales, J. M., Cess, R. D., Coakley, J. A., Hansen, J. E., and
448 Hoffmann, D. J.: Climate forcing by anthropogenic aerosols, *Science*, 255, 423-430, 1992.

449 Chen, Da-Ren, David Y.H. Pui, and Stanley L. Kaufman.: Electro spraying of conducting liquids
450 for monodisperse aerosol generation in the 4 nm to 1.8 nm diameter range, *J. Aerosol Sci.*,
451 26:963-977.

452 Cheng, Y. F., Su, H., Koop, T., Mikhailov, E., and Pöschl, U.: Size dependence of phase transitions
453 in aerosol nanoparticles, *Nat. Commun.*, 6, 5923, doi:10.1038/ncomms6923, 2015.

454 Cheng, Y. F., Su, H., Rose, D., Gunthe, S. S., Berghof, M., Wehner, B., Achtert, P., Nowak, A.,
455 Takegawa, N., Kondo, Y., Shiraiwa, M., Gong, Y. G., Shao, M., Hu, M., Zhu, T., Zhang, Y.
456 H., Carmichael, G. R., Wiedensohler, A., Andreae, M. O., and Pöschl, U.: Size-resolved
457 measurement of the mixing state of soot in the megacity Beijing, China: diurnal cycle, aging
458 and parameterization, *Atmos. Chem. Phys.*, 12, 4477–4491, [https://doi.org/10.5194/acp-12-](https://doi.org/10.5194/acp-12-4477-2012)
459 [4477-2012](https://doi.org/10.5194/acp-12-4477-2012), 2012.

460 Chýlek, P. and Coakley, J. A.: Aerosols and climate, *Science*, 183, 75-77, 1974.

461 Clegg, S. L., Brimblecombe, P., and Wexler, A. S.: Thermodynamic model of the system
462 $\text{H}^+ - \text{NH}_4^+ - \text{SO}_4^{2-} - \text{NO}_3^- - \text{H}_2\text{O}$ at tropospheric temperatures, *J. Phys. Chem. A*, 102, 2137–
463 2154, doi:10.1021/Jp973042r, 1998.

464 Clegg, S. L., Seinfeld, J. H., and Brimblecombe, P.: Thermodynamic modelling of aqueous
465 aerosols containing electrolytes and dissolved organic compounds, *J. Aerosol Sci.*, 32, 713–
466 738, doi:10.1016/s0021-8502(00)00105-1, 2001.

467 Clegg, S. L. and Seinfeld, J. H.: Thermodynamic models of aqueous solutions containing in-
468 organic electrolytes and dicarboxylic acids at 298.15 K. 2. Systems including dissociation
469 equilibria, *J. Phys. Chem. A*, 110, 5718–5734, doi:10.1021/jp056150j, 2006.

470 Comesaña, J. F., Correa, A., and Sereno, A. M.: Water activity at 35 °C in ‘sugar’ + water and
471 ‘sugar’ + sodium chloride + water systems, *Int. J. Food Sci. Tech.*, 36, 655-661, 2001.

472 Dick, W. D., Saxena, P., and McMurry, P. H.: Estimation of water uptake by organic compounds
473 in submicron aerosols measured during the Southeastern Aerosol and Visibility Study, *J. Geo-
474 phys. Res.-Atmos.*, 105, 1471–1479, doi:10.1029/1999jd901001, 2000.

475 Dunne, E. M., Gordon, H., Kürten, A., Almeida, J., Duplissy, J., Williamson, C., Ortega, I. K.,
476 Pringle, K. J., Adamov, A., Baltensperger, U., Barmet, P., Benduhn, F., Bianchi, F.,
477 Breitenlechner, M., Clarke, A., Curtius, J., Dommen, J., Donahue, N. M., Ehrhart, S., Flagan,
478 R. C., Franchin, A., Guida, R., Hakala, J., Hansel, A., Heinritzi, M., Jokinen, T., Kangasluoma,
479 J., Kirkby, J., Kulmala, M., Kupc, A., Lawler, M. J., Lehtipalo, K., Makhmutov, V., Mann,
480 G., Mathot, S., Merikanto, J., Miettinen, P., Nenes, A., Onnela, A., Rap, A., Reddington, C.
481 L. S., Riccobono, F., Richards, N. A. D., Rissanen, M. P., Rondo, L., Sarnela, N.,
482 Schobesberger, S., Sengupta, K., Simon, M., Sipilä, M., Smith, J. N., Stozkhov, Y., Tomé, A.,
483 Tröstl, J., Wagner, P. E., Wimmer, D., Winkler, P. M., Worsnop, D. R., and Carslaw, K. S.:
484 Global atmospheric particle formation from CERN CLOUD measurements, *Science.*, 354,
485 1119-1124, 2016.

486 Duplissy, J., Gysel, M., Sjogren, S., Meyer, N., Good, N., Kammermann, L., Michaud, V., Weigel,
487 R., Martins dos Santos, S., Gruening, C., Villani, P., Laj, P., Sellegri, K., Metzger, A.,
488 McFiggans, G. B., Wehrle, G., Richter, R., Dommen, J., Ristovski, Z., Baltensperger, U., and
489 Weingartner, E.: Intercomparison study of six HTDMAs: results and recommendations,
490 *Atmos. Meas. Tech.*, 2, 363–378, <https://doi.org/10.5194/amt-2-363-2009>, 2009.

491 Dusek, U., Frank, G. P., Curtius, J., Drewnick, F., Schneider, J., Kürten, A., Rose, D., Andreae, M.
492 O., Borrmann, S., and Pöschl, U.: Enhanced organic mass fraction and decreased
493 hygroscopicity of cloud condensation nuclei (CCN) during new particle formation events,
494 *Geophys. Res. Lett.*, 37, 2010.

495 Dutcher, C. S., Ge, X., Wexler, A. S. & Clegg, S. L. An Isotherm-Based Thermodynamic Model
496 of Multicomponent Aqueous Solutions, Applicable Over the Entire Concentration Range. *J.*
497 *Phys. Chem. A* 117, 3198-3213 (2013).

498 Elias, V. O., Simoneit, B. R. T., Cordeiro, R. C., and Turcq, B.: Evaluating levoglucosan as an
499 indicator of biomass burning in Carajás, amazônia: a comparison to the charcoal
500 record22Associate editor: R. Summons, *Geochim. Cosmochim. Acta.*, 65, 267-272, 2001.

501 Estillore, A. D., Morris, H. S., Or, V. W., Lee, H. D., Alves, M. R., Marciano, M. A., Laskina, O.,
502 Qin, Z., Tivanski, A. V., and Grassian, V. H.: Linking hygroscopicity and the surface
503 microstructure of model inorganic salts, simple and complex carbohydrates, and authentic sea
504 spray aerosol particles, *Phys. Chem. Chem. Phys.*, 19, 21101-21111, 2017.

505 Ferreira, O., Brignole, E. A., and Macedo, E. A.: Phase equilibria in sugar solutions using the A-
506 UNIFAC model, *Ind. Eng. Chem. Res.*, 42 (24), 6212–6222, 2003.

507 Fraser, M. P. and Lakshmanan, K.: Using Levoglucosan as a Molecular Marker for the Long-Range
508 Transport of Biomass Combustion Aerosols, *Environ. Sci. Technol.*, 34, 4560-4564, 2000.

509 Fredenslund, A., Jones, R. L., and Prausnitz, J. M.: Group-contribution estimation of activity-
510 coefficients in nonideal liquid-mixtures, *Aiche J.*, 21, 1086–1099, doi:10.1002/aic.690210607,
511 1975.

512 Hämeri, K., Laaksonen, A., Väkevä, M., and Suni, T.: Hygroscopic growth of ultrafine sodium
513 chloride particles, *J. Geophys. Res.*, 106, 20 749–20 757, 2001.

514 Hämeri, K., Väkevä, M., Hansson, H.-C., and Laaksonen, A.: Hygroscopic growth of ultrafine
515 ammonium sulfate aerosol measured using an ultrafine tandem differential mobility analyzer,
516 *J. Geophys. Res.*, 105, 22 231–22 242, 2000.

517 Hansen, H. K., Rasmussen, P., Fredenslund, A., Schiller, M., and Gmehling, J.: Vapor–liquid
518 equilibria by UNIFAC group contribution. 5. Revision and extension, *Ind. Eng. Chem. Res.*,
519 30, 2352–2355, doi:10.1021/ie00058a017, 1991.

520 Hennigan, Christopher J.; Sullivan, Amy P.; Collett, Jeffrey L.; Robinson, Allen L., Levoglucosan
521 stability in biomass burning particles exposed to hydroxyl radicals. *Geophysical Research*
522 *Letters*, 37(9), doi:10.1029/2010gl043088, 2010.

523 Kerminen, V.-M.: The effects of particle chemical character and atmospheric processes on particle
524 hygroscopic properties, *J. Aerosol Sci.*, 28, 121–132, 1997.

525 Keskinen, H., Virtanen, A., Joutsensaari, J., Tsagkogeorgas, G., Duplissy, J., Schobesberger, S.,
526 Gysel, M., Riccobono, F., Slowik, J. G., Bianchi, F., Yli-Juuti, T., Lehtipalo, K., Rondo, L.,
527 Breitenlechner, M., Kupc, A., Almeida, J., Amorim, A., Dunne, E. M., Downard, A. J.,
528 Ehrhart, S., Franchin, A., Kajos, M. K., Kirkby, J., Kürten, A., Nieminen, T., Makhmutov, V.,
529 Mathot, S., Miettinen, P., Onnela, A., Petäjä, T., Praplan, A., Santos, F. D., Schallhart, S.,
530 Sipilä, M., Stozhkov, Y., Tomé, A., Vaattovaara, P., Wimmer, D., Prevot, A., Dommen, J.,
531 Donahue, N. M., Flagan, R. C., Weingartner, E., Viisanen, Y., Riipinen, I., Hansel, A., Curtius,

532 J., Kulmala, M., Worsnop, D. R., Baltensperger, U., Wex, H., Stratmann, F., and Laaksonen,
533 A.: Evolution of particle composition in CLOUD nucleation experiments, *Atmos. Chem.*
534 *Phys.*, 13, 5587–5600, <https://doi.org/10.5194/acp-13-5587-2013>, 2013.

535 Kim, J., Ahlm, L., Yli-Juuti, T., Lawler, M., Keskinen, H., Tröstl, J., Schobesberger, S., Duplissy,
536 J., Amorim, A., Bianchi, F., Donahue, N. M., Flagan, R. C., Hakala, J., Heinritzi, M., Jokinen,
537 T., Kürten, A., Laaksonen, A., Lehtipalo, K., Miettinen, P., Petäjä, T., Rissanen, M. P., Rondo,
538 L., Sengupta, K., Simon, M., Tomé, A., Williamson, C., Wimmer, D., Winkler, P. M., Ehrhart,
539 S., Ye, P., Kirkby, J., Curtius, J., Baltensperger, U., Kulmala, M., Lehtinen, K. E. J., Smith, J.
540 N., Riipinen, I., and Virtanen, A.: Hygroscopicity of nanoparticles produced from
541 homogeneous nucleation in the CLOUD experiments, *Atmos. Chem. Phys.*, 16, 293–304,
542 <https://doi.org/10.5194/acp-16-293-2016>, 2016.

543 Koehler, K. A., Kreidenweis, S. M., DeMott, P. J., Prenni, A. J., Carrico, C. M., Ervens, B., and
544 Feingold, G.: Water activity and activation diameters from hygroscopicity data - Part II:
545 Application to organic species, *Atmos. Chem. Phys.*, 6, 795-809, 2006.

546 Köhler, H.: The nucleus in and the growth of hygroscopic droplets, *Trans. Faraday Soc.*, 32, 1152–
547 1161, 1936.

548 Kreidenweis, S. M., Koehler, K., DeMott, P. J., Prenni, A. J., Carrico, C., and Ervens, B.: Water
549 activity and activation diameters from hygroscopicity data - Part I: Theory and application to
550 inorganic salts, *Atmos. Chem. Phys.*, 5, 1357–1370, <https://doi.org/10.5194/acp-5-1357-2005>,
551 2005.

552 Kulmala, M., Kontkanen, J., Junninen, H., Lehtipalo, K., Manninen, H. E., Nieminen, T., Petäjä,
553 T., Sipilä, M., Schobesberger, S., Rantala, P., Franchin, A., Jokinen, T., Järvinen, E., Äijälä,
554 M., Kangasluoma, J., Hakala, J., Aalto, P. P., Paasonen, P., Mikkilä, J., Vanhanen, J., Aalto,

555 J., Hakola, H., Makkonen, U., Ruuskanen, T., Mauldin, R. L., Duplissy, J., Vehkamäki, H.,
556 Bäck, J., Kortelainen, A., Riipinen, I., Kurtén, T., Johnston, M. V., Smith, J. N., Ehn, M.,
557 Mentel, T. F., Lehtinen, K. E. J., Laaksonen, A., Kerminen, V.-M., and Worsnop, D. R.: Direct
558 Observations of Atmospheric Aerosol Nucleation, *Science*, 339, 943-946, 2013.

559 Lei, T., Ma, N., Hong, J., Tuch, T., Wang, X., Wang, Z., Pöhlker, M., Ge, M., Wang, W., Mikhailov,
560 E., Hoffmann, T., Pöschl, U., Su, H., Wiedensohler, A., and Cheng, Y.: Nano-hygroscopicity
561 tandem differential mobility analyzer (nano-HTDMA) for investigating hygroscopic
562 properties of sub-10 nm aerosol nanoparticles, *Atmos. Meas. Tech.*, 13, 5551–5567,
563 <https://doi.org/10.5194/amt-13-5551-2020>, 2020

564 Lei, T., Zuend, A., Cheng, Y., Su, H., Wang, W., and Ge, M.: Hygroscopicity of organic surrogate
565 compounds from biomass burning and their effect on the efflorescence of ammonium
566 sulfate in mixed aerosol particles, *Atmos. Chem. Phys.*, 18, 1045-1064, 2018.

567 Lei, T., Zuend, A., Wang, W. G., Zhang, Y. H., and Ge, M. F.: Hygroscopicity of organic
568 compounds from biomass burning and their influence on the water uptake of mixed organic
569 ammonium sulfate aerosols, *Atmos. Chem. Phys.*, 14, 11165-11183, 2014.

570 Lihavainen, H., Kerminen, V.-M., Komppula, M., Hatakka, J., Aaltonen, V., Kulmala, M., and
571 Viisanen, Y.: Production of “potential” cloud condensation nuclei associated with
572 atmospheric new-particle formation in northern Finland, *J. Geophys. Res.*, 108, 4782,
573 [doi:10.1029/2003JD003887](https://doi.org/10.1029/2003JD003887), 2003.

574 Mikhailov, E., Vlasenko, S., Martin, S. T., Koop, T., and Pöschl, U.: Amorphous and crystalline
575 aerosol particles interacting with water vapor: conceptual framework and experimental
576 evidence for restructuring, phase transitions and kinetic limitations, *Atmos. Chem. Phys.*, 9,
577 9491–9522, <https://doi.org/10.5194/acp-9-9491-2009>, 2009.

578 Mikhailov, E. F. and Vlasenko, S. S.: High humidity tandem differential mobility analyzer for
579 accurate determination of aerosol hygroscopic growth, microstructure and activity
580 coefficients over a wide range of relative humidity, *Atmos. Meas. Tech.*, 13, 2035–2056,
581 <https://doi.org/10.5194/amt-13-2035-2020>, 2020.

582 Mikhailov, E. F., Vlasenko, S. S., and Ryshkevich, T. I.: Influence of chemical composition and
583 microstructure on the hygroscopic growth of pyrogenic aerosol, *Izv. Atmos. Ocean. Phys.*, 44,
584 416–431, 2008.

585 Mochida, M. and Kawamura, K.: Hygroscopic properties of levoglucosan and related organic
586 compounds characteristic to biomass burning aerosol particles, *J. Geophys. Res.-Atmos.*, 109,
587 D21202, doi:10.1029/2004jd004962, 2004.

588 Peng, C., Chow, A. H. L., and Chan, C. K.: Hygroscopic study of glucose, citric acid, and sorbitol
589 using an electrodynamic balance: comparison with UNIFAC Predictions, *Aerosol Sci.*
590 *Technol.*, 35 (3), 753–758, 2001.

591 Pruppacher, H. R. and Klett, J. D: *Microphysics of clouds and precipitation*, Kluwer Academic
592 Publishers, 1997.

593 Pöhlker, M. L., Pöhlker, C., Ditas, F., Klimach, T., Hrabec de Angelis, I., Araújo, A., Brito, J.,
594 Carbone, S., Cheng, Y., Chi, X., Ditz, 105 R., Gunthe, S. S., Kesselmeier, J., Könemann, T.,
595 Lavrič, J. V., Martin, S. T., Mikhailov, E., Moran-Zuloaga, D., Rose, D., Saturno, J., Su, H.,
596 Thalman, R., Walter, D., Wang, J., Wolff, S., Barbosa, H. M. J., Artaxo, P., Andreae, M. O.,
597 and Pöschl, U.: Longterm observations of cloud condensation nuclei in the Amazon 110 rain
598 forest – Part 1: Aerosol size distribution, hygroscopicity, and new model parametrizations for
599 CCN prediction, *Atmos. Chem. Phys.*, 16, 15709–15740, [https://doi.org/10.5194/acp-16-](https://doi.org/10.5194/acp-16-157092016)
600 157092016, 2016

601 Raoux, S., Rettner, C. T., Jordan-Sweet, J. L., Kellock, A. J., Topuria, T., Rice, P. M., and Miller,
602 D. C.: Direct observation of amorphous to crystalline phase transitions in nanoparticle arrays
603 of phase change materials, *J. Appl. Phys.*, 102, 094305 (2007).

604 Randles, C. A., Russell, L. M., and Ramaswamy, V.: Hygroscopic and optical properties of organic
605 sea salt aerosol and consequences for climate forcing, *Geophys. Res. Lett.*, 31, L16 108,
606 doi:10.1029/2004GL020628, 2004.

607 Seinfeld, J. H., and Pandis, S. N.: *Atmospheric Chemistry and Physics: From Air Pollution to*
608 *Climate Change (Second edition)*, Wiley Interscience, New York, 2006.

609 Sihto, S. L., Mikkilä, J., Vanhanen, J., Ehn, M., Liao, L., Lehtipalo, K., Aalto, P. P., Duplissy, J.,
610 Petäjä, T., Kerminen, V. M., Boy, M., and Kulmala, M.: Seasonal variation of CCN
611 concentrations and aerosol activation properties in boreal forest, *Atmos. Chem. Phys.*, 11,
612 13269-13285, <https://doi.org/10.5194/acp-11-13269-2011>, 2011.

613 Simoneit, B. R. T., Schauer, J. J., Nolte, C. G., Oros, D. R., Elias, V. O., Fraser, M. P., Rogge, W.
614 F., and Cass, G. R.: Levoglucosan, a tracer for cellulose in biomass burning and atmospheric
615 particles, *Atmos. Environ*, 33, 173-182, 1999.

616 Suda, S. R. and Petters, M. D.: Accurate determination of aerosol activity coefficients at relative
617 humidities up to 99 % using the hygroscopicity tandem differential mobility analyzer
618 technique, *Aerosol Sci. Technol.*, 47, 991–
619 1000, <https://doi.org/10.1080/02786826.2013.807906>, 2013.

620 Su, H., Rose, D., Cheng, Y. F., Gunthe, S. S., Massling, A., Stock, M., Wiedensohler, A., Andreae,
621 M. O., and Pöschl, U.: Hygroscopicity distribution concept for measurement data analysis and
622 modeling of aerosol particle mixing state with regard to hygroscopic growth and CCN

623 activation, *Atmos. Chem. Phys.*, 10, 7489–7503, <https://doi.org/10.5194/acp-10-7489-2010>,
624 2010.

625 Svenningsson, B., Rissler, J., Swietlicki, E., Mircea, M., Bilde, M., Facchini, M. C., Decesari, S.,
626 Fuzzi, S., Zhou, J., Mønster, J., and Rosenørn, T.: Hygroscopic growth and critical
627 supersaturations for mixed aerosol particles of inorganic and organic compounds of
628 atmospheric relevance, *Atmos. Chem. Phys.*, 6, 1937-1952, 2006.

629 Tang, I. N.: Chemical and size effects of hygroscopic aerosols on light scattering coefficients, *J.*
630 *Geophys. Res.*, 101, 19 245– 19 250, 1996.

631 Tang, I. N., Fung, K. H., Imre, D. G., and Munkelwitz, H. R.: Phase Transformation and
632 Metastability of Hygroscopic Microparticles, *J. Geophys. Res.-Atmos*, 99, 18801– 18808,
633 1994.

634 Wang, J., Shilling, J. E., Liu, J., Zelenyuk, A., Bell, D. M., Petters, M. D., Thalman, R., Mei, F.,
635 Zaveri, R. A., and Zheng, G.: Cloud droplet activation of secondary organic aerosol is mainly
636 controlled by molecular weight, not water solubility, *Atmos. Chem. Phys.*, 19, 941-954, 2019.

637 Wang, Z., Cheng, Y., Ma, N., Mikhailov, E., Pöschl, U., and Su, H.: Dependence of the
638 hygroscopicity parameter κ on particle size, humidity and solute concentration: implications
639 for laboratory experiments, field measurements and model studies, *Atmos. Chem. Phys.*
640 *Discuss.*, 2017, 1-33, 2017.

641 Wang, Z., Su, H., Wang, X., Ma, N., Wiedensohler, A., Pöschl, U., and Cheng, Y.: Scanning
642 supersaturation condensation particle counter applied as a nano-CCN counter for size-
643 resolved analysis of the hygroscopicity and chemical composition of nanoparticles, *Atmos.*
644 *Meas. Tech.*, 8, 2161–2172, <https://doi.org/10.5194/amt-8-2161-2015>, 2015.

645 Wiedensohler, A., Cheng, Y. F., Nowak, A., Wehner, B., Achtert, P., Berghof, M., Birmili, W.,
646 Wu, Z. J., Hu, M., Zhu, T., Takegawa, N., Kita, K., Kondo, Y., Lou, S. R., Hofzumahaus, A.,
647 Holland, F., Wahner, A., Gunthe, S. S., Rose, D., Su, H., and Pöschl, U.: Rapid aerosol particle
648 growth and increase of cloud condensation nucleus activity by secondary aerosol formation
649 and condensation: A case study for regional air pollution in northeastern China, *J. Geophys.*
650 *Res.–Atmos.*, 114, doi:10.1029/2008JD010884, 2009.

651 Wiedensohler, A., Lütke-meier, E., Feldpausch, M., & Helsper, C. (1986). Investigation of the
652 bipolar charge distribution at various gas conditions. *J. Aerosol Sci.*, 17(3), 413–416.
653 [https://doi.org/10.1016/0021-8502\(86\)90118-7](https://doi.org/10.1016/0021-8502(86)90118-7).

654 Zhang, R.: Getting to the Critical Nucleus of Aerosol Formation, *Science*, 328, 1366-1367, 2010.

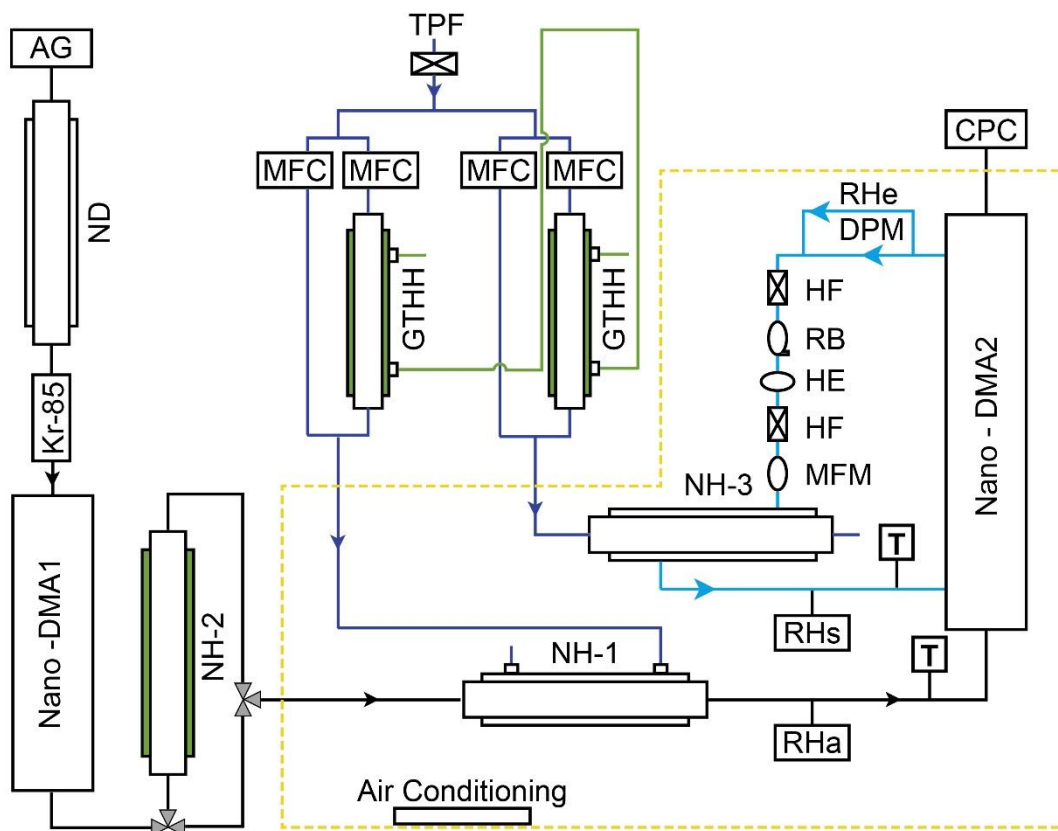
655 Zhang, R., Khalizov, A., Wang, L., Hu, M., and Xu, W.: Nucleation and Growth of Nanoparticles
656 in the Atmosphere, *Chem. Re.*, 112, 1957-2011, 2012.

657 Zhang, R., Suh, I., Zhao, J., Zhang, D., Fortner, E. C., Tie, X., Molina, L. T., and Molina, M. J.:
658 Atmospheric New Particle Formation Enhanced by Organic Acids, *Science*, 304, 1487-1490,
659 2004.

660 Zamora, I., Tabazadeh, A., Golden, D., and Jacobson, M.: Hygroscopic growth of common organic
661 aerosol solutes, including humic substances, as derived from water activity measurements,
662 *Journal of Geophysical Research (Atmospheres)*, 116, 23207, 10.1029/2011JD016067, 2011.

663 Zieger, P., Fierz-Schmidhauser, R., Weingartner, E., and Baltensperger, U.: Effects of relative
664 humidity on aerosol light scattering: results from different European sites, *Atmos. Chem.*
665 *Phys.*, 13, 10609–10631, <https://doi.org/10.5194/acp-13-10609-2013>, 2013.

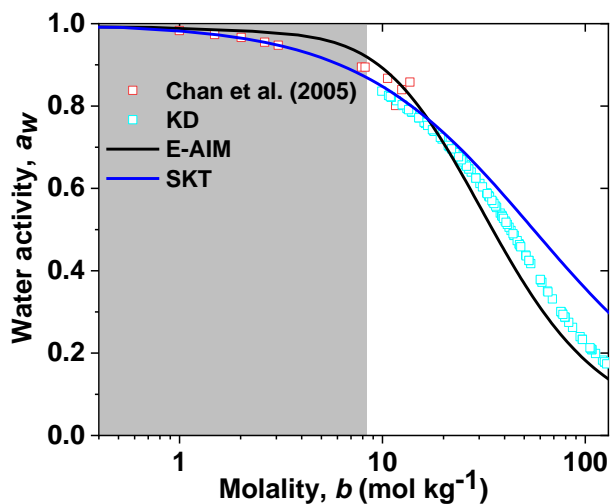
666



667
 668 **Figure 1.** Experimental setup of the nano-HTDMA. Here, AG: aerosol generator (aerosol atomizer or electrospray);
 669 ND: nafion dryer; Kr-85: Krypton source aerosol neutralizer; Nano-DMA: nano differential mobility analyzer; TPF:
 670 total particle filter; HF: hydrophobic filter; MFC: mass flow controller; MFM: mass flow meter; RB: recirculation
 671 blower; DPM: dew point mirror; GTHH: Gore-Tex humidifier and heater; NH: nafion humidifier; HE: heat exchanger;
 672 CPC: condensation particle counter; Black line: aerosol line; Blue line: sheath line; Royal blue line: humidified air;
 673 Green line: MilliQ water (resistivity of 18.2 MΩ cm at 298.15 K). RH_a and RH_s (measured by RH sensors) represent
 674 the RH of aerosol and sheath flow in the inlet of nano-DMA2, respectively. RH_e (measured by dew point) represents
 675 the RH of excess air. T represent the temperature of aerosol and sheath flow in the inlet of nano-DMA2, respectively.

676
 677
 678
 679
 680

681



682

683 **Figure 2.** Concentration-dependent water activity (a_w) of levoglucosan solution. The KD-derived a_w (KD=Kreidenweis,
684 cyan open square) is compared with observations (red open square), E-AIM (Extend-Aerosol Inorganic Model, black
685 line), and a_w model (SKT, blue line). The light grey shaded areas mark the sub-saturated concentration with respect to
686 bulk solution.

687

688

689

690

691

692

693

694

695

696

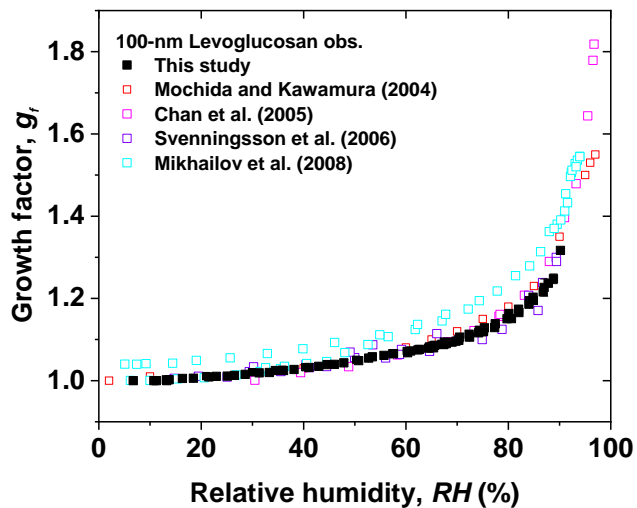
697

698

699

700

701



702

703 **Figure 3.** Hygroscopic diameter growth factor (G_f) of levoglucosan particles with dry diameter of 100 nm in both
704 deliquescence and efflorescence mode processes (black solid square). The measured data compared with literature data
705 from Mochida and Kawamura (2004) in both deliquescence and efflorescence modes (red open square), Chan et al.
706 (2005) in the deliquescence mode (magenta open square), Svenningsson et al. (2006) in the deliquescence mode (violet
707 open square), and Mikhailov et al. (2008) in both deliquescence and efflorescence modes (cyan open square).

708

709

710

711

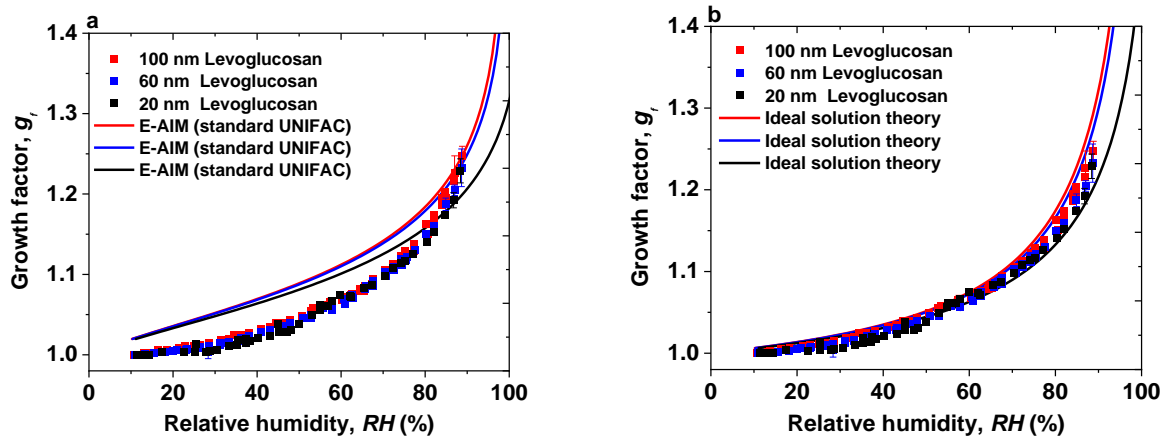
712

713

714

715

716



717

718 **Figure 4.** Hygroscopic diameter growth factor (G_f) of levoglucosan particles with dry diameter of 100 nm (red square),

719 60 nm (blue square), and 20nm (green square). Köhler model curves are based on: (a) E-AIM (standard UNIFAC)

720 (100 nm: red, 60 nm: blue, 20 nm: green line), (b) ideal solution theory (100 nm: red, 60 nm: blue, 20 nm: green line).

721

722

723

724

725

726

727

728

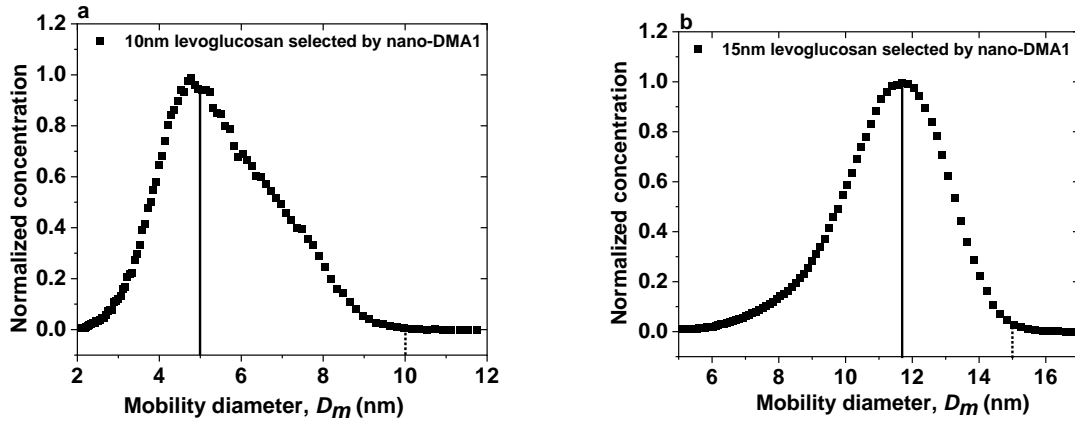
729

730

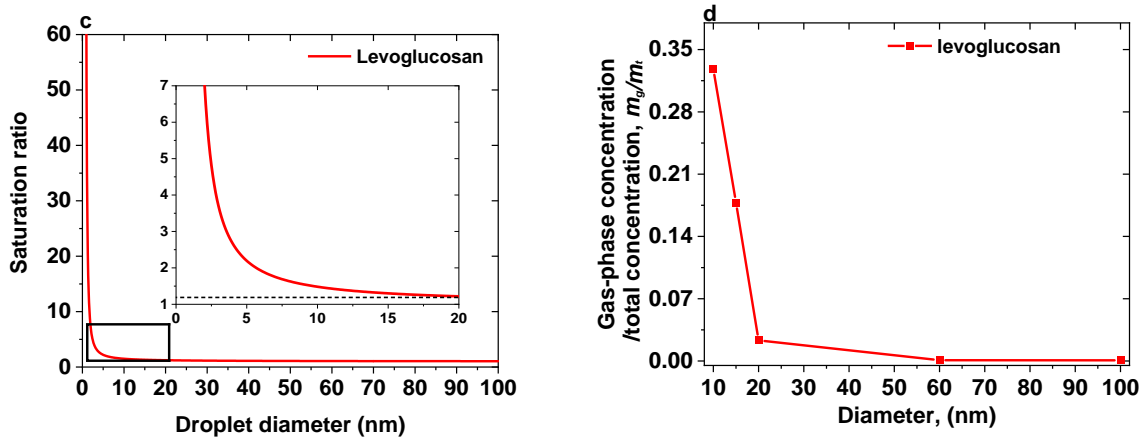
731

732

733



734



735

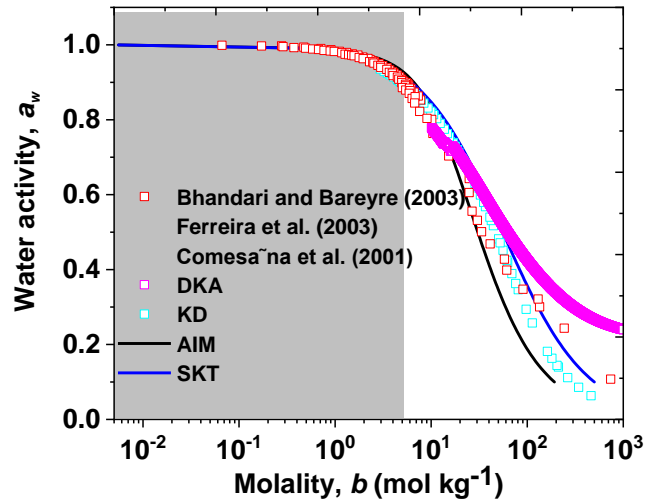
736 **Figure 5.** The normalized size distributions scanned by nano-DMA2 for: (a) 10 nm and (b) 15-nm levoglucosan at 10%
737 at 298K. The dotted lines mark the diameters of the monodispersed nanoparticles selected by the nano-DMA1. The
738 back solid lines mark the peak diameters from the normalized size distributions scanned by the nano-DMA2. (c) Vapor
739 saturation ratio of levoglucosan as a function of nanodroplet diameter according to the Kelvin equation. The diameter
740 range 0-20 nm for the saturation ratio of levoglucosan particles is shown as an inset. The value of surface tension of
741 pure levoglucosan is 0.0227104 [J m⁻²]. (d) The ratio of gas-phase concentration (m_g) to the total concentration (m_t) of
742 levoglucosan nanoparticles against diameter.

743

744

745

746



747

748 **Figure 6.** Concentration-dependent water activity (a_w) of D-glucose solution. The DKA-derived a_w (Differential
749 Köhler Analysis, magenta open square) is compared with observations (red open square), E-AIM (Extend-Aerosol
750 Inorganic Model, black line), a_w model (SKT, blue line), and parameterization model for a_w (KD=Kreidenweis, cyan
751 open square). The light grey shaded areas mark the sub-saturated concentration with respect to bulk solution.

752

753

754

755

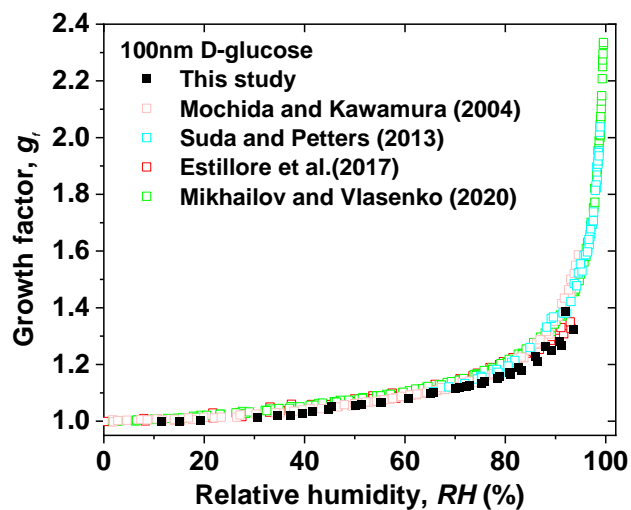
756

757

758

759

760



761

762 **Figure 7.** Hygroscopic diameter growth factor (G_f) of D-glucose particles with dry diameter of 100 nm in both
763 deliquescence and efflorescence modes (black solid square). The measured data compared with reference data from
764 Mochida and Kawamura (2004) in both deliquescence and efflorescence modes (pink open square), Suda and Petters,
765 (20017) in deliquescence mode (violet open square), Estillore et al., (2017) in both deliquescence and efflorescence
766 modes (red open square), and Mikhailov and Vlasenko (2020) in both deliquescence and efflorescence modes (green
767 open square).

768

769

770

771

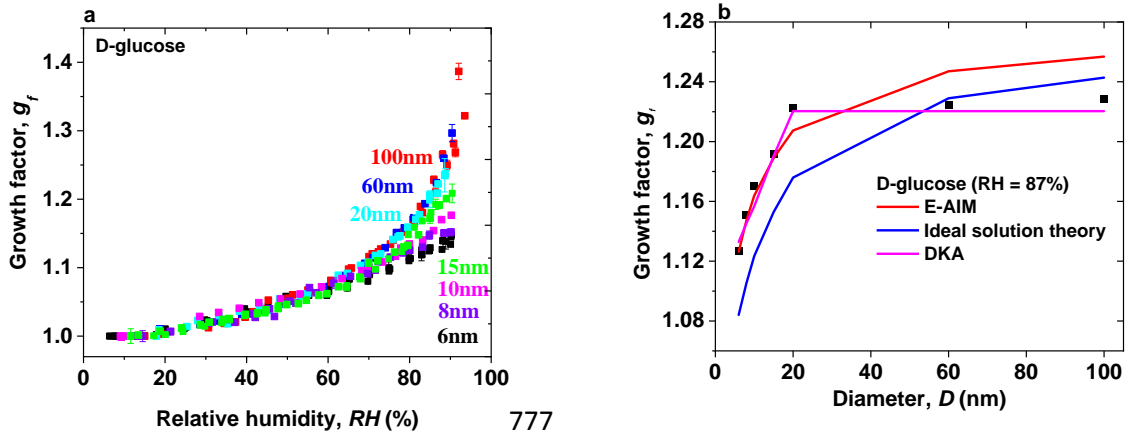
772

773

774

775

776



778 **Figure 8.** (a) Hygroscopic diameter growth factor (G_f) of D-glucose nanoparticles with dry diameters of 100 nm (red
779 square), 60 nm (blue square), 20 nm (cyan square), 15 nm (green square), 10 nm (pink square), 8 nm (royal square),
780 and 6 nm (black square). (b) Hygroscopic diameter growth factor (G_f , black square) of D-glucose nanoparticles with
781 dry diameters from 6 to 100 nm at 87% RH. The measured hygroscopic growth factors of D-glucose nanoparticles
782 with diameters from 100 down to are compared with E-AIM model (red line), ideal solution theory (blue line), and
783 DKA prediction (pink line).

784

785

786

787

788

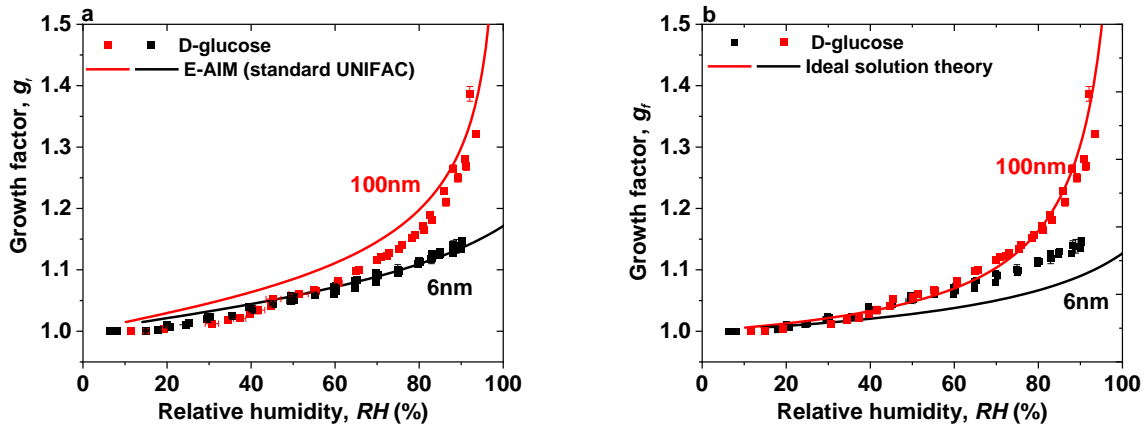
789

790

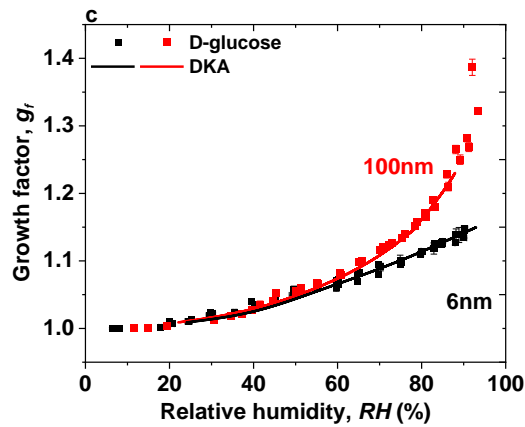
791

792

793



794



795

796 **Figure 9.** Hygroscopic diameter growth factor (G_r) of D-glucose nanoparticles with dry diameters of 100 nm (red
797 square) and 6 nm (black square). Köhler model curves are based on: (a) AIM (standard UNIFAC), (100 nm: red, 6 nm:
798 black line), (b) ideal solution theory (100 nm: red, 6 nm: black line), and (c) DKA mode (100 nm: red, 6 nm: black
799 line).